



Effect of carbonation on the hydro-mechanical properties of Portland cements

A. Fabbri^{a,*}, J. Corvisier^a, A. Schubnel^a, F. Brunet^a, B. Goffé^a, G. Rimmelle^b, V. Barlet-Gouédard^b

^a *Laboratoire de Géologie, UMR 8538 ENS – CNRS, 24, rue Lhomond, 75005 Paris, France*

corvisier@geologie.ens.fr, aschubnel@geologie.ens.fr, brunet@geologie.ens.fr, goffe@geologie.ens.fr

^b *Schlumberger Riboud Product Center (SRPC), 1 Rue Becquerel, BP 202, F-92142 Clamart, France*

grimmele@clamart.oilfield.slb.com, vbarlet@clamart.oilfield.slb.com

* *Corresponding author. New address: BRGM – GEO/G2R, 3, avenue Claude Guillemin, 45060 Orléans Cedex 2, France. a.fabbri@brgm.fr*

ABSTRACT.

We evaluate experimentally the effect of carbonation on the hydro-mechanical properties of Portland cement. Samples were carbonated at 90°C and 28MPa under wet supercritical CO₂. Two types of carbonation features were achieved, either the samples were homogeneously carbonated or they displayed sharp carbonation fronts. Using a tri-axial apparatus, the static elastic moduli and the mechanical strength were measured at in-situ pressure conditions (28MPa) and showed a degradation of the mechanical properties of the samples where a carbonation front prevailed. Water and gas permeabilities were measured and showed that the samples with a carbonation front exhibit a stress sensitive permeability. P and S elastic wave velocities were measured to evaluate dynamic (ultrasonic range, 1 MHz) elastic moduli. The use of an effective medium theory approach enabled us to characterize the density and distribution of cracks within the samples. This approach outlines that the samples which developed a carbonation front were damaged.

KEY WORDS: Characterisation (B), Microcracking (B), Carbonation (C), Elastic Moduli (C), Permeability (C).

1. Introduction

Underground CO₂ sequestration may be considered as an effective option only if the long-term integrity of the reservoirs can be insured. In this context, carbonation induced failure of the well-bore cement may create preferential carbon dioxide migration pathways back to the surface. The interaction between carbon dioxide and Portland cement at atmospheric pressure and temperature conditions is a relatively well-known phenomenon since it leads to the carbonation of the cement matrix and the corrosion of the reinforcements embedded in concrete (e.g., [1]). Especially, the mechanical strength and the elastic moduli of the cementitious matrix are known to increase significantly [2-4]. However, in the context of deep geological storage, elevated temperatures and high carbon dioxide concentrations will be encountered concurrently which might potentially enhance the chemical corrosion of Portland cement [5-10]. In particular, the interaction between cement and wet supercritical CO₂ (wet scCO₂) and/or CO₂ dissolved in water is expected to change significantly the mechanical behaviour of the hardened cement paste.

In this paper, we propose a quantitative mechanical post-characterization of Portland cement samples exposed to 90°C, 28 MPa and wet scCO₂ at several test durations. Using a tri-axial apparatus, static elastic moduli, P and S elastic wave velocities measurements (ultrasonic range, 1MHz) and gas/water permeabilities were measured under confining pressure and deviatoric load, in dry and saturated conditions. The set of Portland cement samples were first submitted to wet scCO₂ beforehand within an autoclave under pressure and temperature, whereas subsequent tri-axial testing was carried out at room temperature. An effective medium model developed by Fortin *et al.* [11] is used to interpret qualitatively the mechanical behaviour of the experimentally carbonated cement samples.

2. Experimental methods

2.1. Sample preparation

Cement slurry, with 0.44 water/cement ratio by mass (W/C), was vacuum-mixed according to API specification 10, section 5. Conventional Portland cement, similar to ASTM type I, and fresh water were used. Before mixing the slurry, an anti foam agent, a dispersant and a retarder were added to water in order to optimize the main slurry properties. The cement was cast into 75mm-diameter cylindrical moulds and cured for 72 hours at 20.68 MPa and 90°C in a curing chamber at SRPC (Clamart, France). Then, the specimens were cored and cut into cylindrical samples of 65-mm length and 30-mm diameter. Prior to the exposure to wet scCO₂, half of them were stored in fresh water (index w) while the other half was dried during a week in an oven at 85°C +/- 5°C (index d). Four sets of carbonated samples were obtained after a carbonation process that lasted 13, 35, 51, and 62 days at 28 MPa and 90°C respectively. The experimental set-up used here for cement carbonation under static conditions is described precisely in [8]. The conditions of 28 MPa and 90°C have been chosen for their relevance to deep geological storage. Hardened cement samples (2 dried and 2 wet samples) were positioned in the upper part of the autoclave in a wet supercritical CO₂ environment. They are supported by samples immersed in water which are not studied here (cf. **Figure 1**). At the end of the carbonation stage, the depressurization phase starts from 28 MPa down to 5 MPa in 6 hours and from 5 MPa to atmospheric pressure in 1 hour.

2.2. Experimental set-up

After the carbonation process and prior to the tri-axial testing, core sample surfaces were rectified and polished to ensure perfect parallelism and minimum friction. The samples were dried in an oven at $85^{\circ}\text{C} \pm 5^{\circ}\text{C}$ until they reached a constant mass. They were then kept dried in a hermetic bell jar. Longitudinal and orthoradial strains (noted ε_{zz} and $\varepsilon_{\theta\theta}$ respectively) were measured using strain gauges (TML FLA-20, Tokyosokki) glued directly onto the sample surface. Seven piezoelectric transducers (PI ceramic PI255, 1MHz resonance) were also glued on the cylindrical sample in order to measure two different P, and two different S ultrasonic wave velocities. The schematic representation of the specimen set-up is reported in **Figure 2**. In the following, we did not investigate elastic wave anisotropy and only average P and S velocities will be discussed. Velocities were calculated measuring the time of flight needed for an acoustic pulse to travel across the sample. For each measurement, 100 waveforms were stacked on a digital oscilloscope, in order to increase the signal/noise ratio. The software InSite (ASC Ltd.) was used to monitor and process the digital waveforms. In particular, the arrival time was estimated using a cross-correlation technique. In such conditions, the absolute arrival time error was of the order of a few percents, but the relative error between the master velocity survey and the following ones was lowered to $\sim 0.1\%$. Waveforms of the dried non-carbonated sample under a confining pressure of 30 MPa were chosen as our master survey reference for cross-correlation.

Water and argon gas permeabilities were measured using the constant flow technique provided by a high precision double microvolumetric pump (Quizix Qx20k). Applying a constant pressure difference ($\Delta p = 1$ MPa) at the top and bottom of the sample, the flow through the specimen was calculated from the volume variation of the pumps ($Q = dV_{\text{pump}}/dt$). When the upstream and downstream flow became equal (about 1/2 hour for gas and 2 hours for water), the steady state was supposed to be reached and permeability was estimated using Darcy's law:

$$\kappa = \frac{Q\eta l}{S\Delta p} \quad (1)$$

where η is the viscosity of the fluid (at 20°C and 28 MPa, $\eta = 1.02$ mPa.s for water and $\eta = 30.8$ μ Pa.s for argon gas; [12]), l the specimen length, and S its cross-sectional area. Switching the flow direction in the sample, two symmetrical measurements were systematically performed.

The tri-axial cell at the Laboratoire de Geologie at ENS was previously precisely described in [13-14]. The standard test procedure started with a confining pressure ($\sigma_c = \sigma_{ii}/3$) load, from 0 to 30 MPa. During this confinement stage, the evolution of the dynamic bulk (K) and shear (G) moduli were monitored using the evolution the P and the S elastic wave velocities (V_p and V_s respectively):

$$G = \rho_d V_s^2 \quad \text{and} \quad K = \rho_d \left(V_p^2 - \frac{4}{3} V_s^2 \right) \quad (2)$$

At a confining pressure of 30 MPa, an axial deviatoric stress loading ($\sigma_d = \sigma_{zz} - \sigma_c$), from 0 to 30 MPa, was applied. This led to the estimation of the dry Young's modulus $E_d = 9KG/(3K+G)$ and Poisson's ratio $\nu_d = (3K-2G)/(6K+2G)$ through:

$$E_d = -\left. \frac{\partial \sigma_d}{\partial \varepsilon_{zz}} \right|_{\sigma_c} \quad \text{and} \quad \nu_d = -\left. \frac{\partial \varepsilon_{\theta\theta}}{\partial \varepsilon_{zz}} \right|_{\sigma_c} \quad (3)$$

These two moduli were also estimated in the dynamic range, from ultrasonic velocities (index u in **Table 2**).

In a second stage, the deviatoric stress was unloaded and the argon pore pressure was progressively increased and stabilized to 28 MPa for at least 2 hours, in order to reach a full saturation allowing for gas permeability measurements. The next step consisted in the sample water saturation at a pore pressure of 28 MPa which required at least 12 hours. Applying an increasing axial deviatoric stress, the specimen was eventually loaded to failure. Drained elastic constant E_w and ν_w were estimated and the water permeability was measured at 0 MPa, 30 MPa and 50 MPa axial deviatoric stresses. At the end of each experiment, the sample was carefully unloaded in order to analyze the fracture geometry.

3. Experimental results and discussion

3.1. Results of sample carbonation

As expected, the wet samples led to annular carbonation (AC) with a sharp carbonation front. Typical of a diffusion front, the thickness of the carbonated rim increases linearly with the square root of time [7-8]. However, as shown in **Figure 3**, the previously dried specimens show homogeneous carbonation (HC) through the whole sample, i.e. with no visible front. Since

carbonation fronts arise from a diffusion limited process, homogeneous carbonation can be understood by a rapid diffusion of wet scCO_2 throughout the porous network.

Mineral characterization and porosity distribution in AC cement samples exposed to CO_2 fluids under pressure and temperature have already been the subject of intensive studies [5, 8, 15] and only HC samples will be further characterized here using Raman micro-spectrometry (Renishaw InVia using a 785 nm IR diode laser at ENS) and scanning electron microprobe (Hitachi S-2500 equipped with EDS at ENS) on polished sections as well as X-ray powder diffraction (XRPD, Rigaku, rotating Cu-anode at ENS). The carbonation features in HC samples are roughly similar to those described in the carbonated zone for AC cement: portlandite is carbonated and calcium silicate hydrates (CSH) have transformed into Ca-carbonates and a silica-rich phase (Figure 3). Nevertheless, XRPD data indicate partial carbonation since very low amount of portlandite, occurring as relict, is detected after 35 and 65 days of experimental carbonation (Figure 4). Furthermore, the microtexture of HC samples is different to that of AC (Figure 4). Both XRPD and Raman microspectrometry clearly show that contrarily to AC samples, CaCO_3 -vaterite is not preserved (or has not nucleated) in HC samples and only calcite and aragonite are observed (Figure 5).

Density, water porosity and carbonation-front thickness (when present) of our samples are summarized in Table 1 where t_c is the carbonation time, ϕ is the water porosity (evaluated from the sample mass difference between dried, at $85 \pm 5^\circ\text{C}$, and saturated states), ρ_d is the density of the dried specimen and e_c is the thickness of the carbonation front. This Table highlights that the carbonation process leads to a reduction of porosity and an increase of dried density, which thus shows that both mass and volume of the carbonates which precipitate are higher than the one of the dissolved and/or leached cement solid matrix.

3.2. Mechanical characterisation tests results

The evolutions of elastic wave velocities and the resulting K and G moduli during the confinement stage in dry conditions are reported in **Figures 6A, 6B and 6C** respectively. No significant variations were observed on non-carbonated (PO) and HC samples (P35d, P62d). In contrast, the elastic wave velocities and the K and G moduli of AC (P13w, P51w and P62w) samples revealed significant pressure sensitivity up to a critical pressure (p_c) of approximately 15 MPa. In rock physics, such a pressure sensitivity of the dynamic elastic moduli is commonly interpreted as due to the elastic closure of micro-cracks. Indeed, at a given confining pressure (p_c), all crack of aspect ratio lower than $\zeta = w / c \propto p_c / E$ [16] are expected to be closed. Here, E is the cement matrix Young's modulus, w the crack average half-aperture, and c the crack distribution average radius. In that case, at a confinement pressure of 15 MPa, all cracks of aspect ratio lower than 10^{-3} should be closed under the effect of the confining pressure.

Commonly, elastic wave velocity and dynamic elastic moduli evolution can be interpreted in terms of porosity and crack density (d_f) using an effective medium theory approach. Numerous models exist in the literature (e.g. [17-18]), but one of the simplest cases is that of the non-interactive approach, where stress and strain interactions between inclusions are neglected. Although such an approximation is valid for low porosities and crack densities only, it might be particularly well suited for the case of damaged cements, where such a dual porosity is likely to prevail. This technique has the advantage to separate the effects on the elastic properties of the compliant porosity (i.e. cracks which close under the effect of pressure) and the non-compliant (equate pores that are pressure insensitive). Using such a framework and assuming penny-shaped geometry for the cracks, Fortin *et al.*, [11] showed that the bulk and shear effective moduli of a material could be rigorously expressed in terms of the material's matrix elastic properties, a scalar accounting for crack density and the porosity only :

$$\frac{K_m}{K} = 1 + \frac{d_f}{1-\phi} \frac{h(2-v_m)}{2(1-2v_m)} + \frac{\phi}{1-\phi} \frac{3(1-v_m)}{2(1-2v_m)} \quad (4a)$$

$$\frac{G_m}{G} = 1 + \frac{d_f}{1-\phi} \frac{h(5-v_m)}{5(1-2v_m)} + \frac{\phi}{1-\phi} \frac{15(1-v_m)}{7-5v_m} \quad (4b)$$

where $K_m = K_{30}(1 + (3/2) \phi/(1-\phi) (1-v_m)/(1-2v_m))$, $G_m = G_{30}(1 + 15\phi/(1-\phi) (1-v_m)/(7-5v_m))$, $v_m = (3K_m - 2G_m)/(6K_m + 2G_m)$ and $h = 16(1-v_m^2)/9/(1-0.5v_m)$. The crack density is a scalar defined by

$$\rho = \frac{1}{V} \sum_0^N c_i^3$$

where c_i is the radius of the i^{th} crack, N being the total number of cracks embedded in the representative elementary volume V . For a distribution of penny shaped cracks with constant aspect ratio, the total micro-crack porosity can be expressed as $\phi_{mc} = \pi\rho w/c$. K_{30} and G_{30} are respectively the bulk and the shear modulus of the intact specimen. For sake of simplicity, we assume these to be equal as the moduli measured at 30 MPa confining pressure. The crack density variation is then reported in **Figure 6D**. The d_f values of AC samples at $-\sigma_c = 2$ MPa, ranges from 0.3 to 0.5. The permeability percolation threshold being reached at crack densities of 0.14 only (Guéguen and Palciauskas, 1994), this last observation leads us to the conclusion that, at this low confinement, micro-cracks network are likely to become an important pathway for CO₂ migration. This is not the case for non-carbonated and HC samples where d_f always remains lower than 0.1.

The results of hydro-mechanical characterization are reported in **Figures 7A and 7C** for HC samples, in **Figures 7B and 7D** for AC samples and summarized in **Table 2**. Whatever the characterization test (dry tri-axial, drained tri-axial or dry ultrasonic), the Young's modulus of HC samples (P35d and P62d) are significantly higher than those of the non-carbonated samples. This result is in agreement with former studies which have shown an increase of cement

Young's modulus due to carbonation [4]. However, the Young's modulus of AC samples remains close to those of uncarbonated samples (except for P13w). For the drained saturated case, the Young modulus of all AC samples is even lower than that of uncarbonated samples. In light of the microtextural data on AC cements [5, 8], this feature may be explained by the presence of a dissolution zone (high porosity) just beyond the carbonation front. It is expected that cracks should easily nucleate at the corresponding interface, because of elastic strain incompatibilities between two media of different compliance. The increase of pore pressure could then re-open these cracks which were closed during the confining stage. In this case, the difference in Young's modulus between AC and HC samples is commonly more pronounced under drained saturated conditions than under dry conditions.

Water (κ_w) and gas (κ_{gr}) permeabilities measurements are reported in **Table 1**. For the AC samples, the permeability decreases as the carbonation front thickness increases and the variation between P13w, P35w and P62w samples seems to be linear with the ratio of the carbonated cross-surface. However, in contrast to non-carbonated and HC samples, the application of a deviatoric load was found to increase significantly the permeability (**Figure 8A**). A difference is observed between the gas and water permeabilities (κ_w/κ_{gr} is about 7 for the sound sample and about 2.5 for carbonated samples). It is commonly attributed to the differences between water/solid and gas/solid interactions, slip effects during gas permeability measurement, etc...[19]. As the leaching of the cement matrix and the carbonate precipitation act on these physico-chemical processes, it is not surprising that the difference between κ_w and κ_{gr} is not the same for all the samples. As a consequence, the permeability of carbonated cements under downhole conditions is likely to be stress sensitive and in cases where a deviatoric stress is present, the permeability of the cement can be higher than expected. This result is consistent with the failure shape of the tested samples (cf. **Figure 8B**). Indeed, while the non-carbonated sample exhibits 45° oriented cross fractures commonly observed during tri-

axial loading experiments, the AC samples reveal vertical fractures surrounding the carbonation front. Finally, summarized on Table 1, the strength (f_{rupt}) of AC samples is lower than that of the uncarbonated cement. This is not the case for the HC samples for which no clear tendency is observed: the P35d paste revealed strength of 80 MPa while P62d failed at 57 MPa deviatoric stress.

3.3. Discussion

All these results indicate that AC samples were damaged during or after the carbonation process at 28 MPa. Crack formation in the course of depressurisation of the autoclave after carbonation at 28 MPa cannot be ruled out. One can then wonder why AC samples were much more damaged than HC samples, although they were submitted to the same de-pressurization procedure. This significant increase of the porous space localized at the carbonation front has been also observed by Rimmele *et al.*, [5] and Corvisier *et al.* [15]. This may be due to the stiffness contrast between the carbonated and the dissolution zones in AC samples, at the interface of which cracks (and failure) are expected to occur. Another possibility being that fracturing could occur as a response to the carbonation process itself. Schematically, this process can be divided into two major steps: (1) the dissolution of the cement matrix by the acidic CO₂-rich fluid and (2) carbonate precipitation. Reaction (1) engenders water production and an increase of porosity whereas overall reaction (2) produces a global reduction of porosity, because the carbonate volume is higher than the volume of the cement phases which are consumed. If the precipitation process is fast enough and localised, a significant pore overpressure could happen concurrently and induce damage of the solid matrix. It is here emphasized that damage will increase with decreasing density of the carbonate precipitate. It is then consistent with the fact that vaterite (with a density of 2.5 g/cm³) is observed on the damaged carbonated front of AC samples while only calcite and aragonite (with a density of 2.7

g/cm³ and 2.9 g/cm³, respectively) are observed on less-damaged HC samples. However, as demonstrated in [20], more information on the dissolution and precipitation chemical kinetics is however required to conclude on this point.

4. Conclusion

The static and dynamic elastic constants, as well as water and gas permeabilities of a set of Portland cement samples carbonated under wet scCO₂ at 90degC and 28 MPa were measured at room temperature. The results clearly show a significant pressure sensitivity of these properties in the samples which develop a carbonation front. This can only be interpreted by the presence of micro-cracks. These micro-cracks, which most likely develop in the vicinity of the front, induce a degradation of the mechanical properties of cement, a decrease in its mechanical strength and an increase of its permeability when deviatoric stress is present. Since under real injection conditions, well-bore cements are expected to carbonate with a progressing carbonation front [8, 21], the duration of this transient process appears to be a critical issue both for the cement sealing efficiency and for the long-term well-bore casing integrity. In such a way, elastic wave velocity monitoring of the borehole casings could become an efficient tool to survey the well-bore integrity and predict the evolution of its permeability [22-23].

Acknowledgement: This study was supported by the Agence Nationale de la Recherche in the framework of the COSMOS1 project (...Eurogia...).

References

- [1] T. Chaussadent, Etat des lieux et réflexions sur la carbonatation du béton armé. Etudes et recherches des Laboratoires des Ponts et Chaussées, 1999.
- [2] M. Fernandez Bertos, S. Simons, C. Hills, P. Carey, A review of accelerated carbonation technology in the treatment of cement-based materials and sequestration of CO₂, *Journal of Hazardous Materials B112* (2004) 193-205
- [3] J. Jerga, Physico-mechanical properties of carbonated concrete, *Construction and Buildings Materials* 18 (2004) 645-652.
- [4] J. Xiao, J. Li, B. Zhu, Z. Fan, Experimental study on strength and ductility of carbonated concrete elements, *Construction and Buildings Materials* (2002).
- [5] G. Rimmelé, V. Barlet-Gouédard, O. Porcherie, B. Goffé, F. Brunet, Heterogeneous porosity distribution in Portland cement exposed to CO₂-rich fluids, *Cement and Concrete Research*, Vol. 38 (2008) 1038-1048.
- [6] N. Jacquemet, J. Pironon, J. Saint-Marc, Mineralogical changes of a well cement in various H₂S-CO₂(-brine) fluids at high pressure and temperature, *Environmental Science & Technology* 42, (2008) 282-288.
- [7] J. Corvisier, A. Fabbri, F. Brunet, B. Goffé, V. Barlet-Gouédard, A model for CO₂ wells ageing through water/supercritical CO₂/cement interactions, *Proceedings of the 3rd International Conference on coupled T-H-C-M processes in Geo-Systems*, 2008.
- [8] V. Barlet-Gouédard, G. Rimmelé, B. Goffé, O. Porcherie, Well Technologies for CO₂ Geological Storage: CO₂-Resistant Cement, *Oil & Gas Science and Technology* 62 (2007) 325-334.
- [9] R.A. Bruckdorfer, Carbon dioxide corrosion in oilwell cements, *SPE 15176 Billings, MT*, May 19–21, 1986.
- [10] D.D. Onan, Effects of supercritical carbon dioxide on well cements, *SPE 12593, Permian Basin Oil & gas recovery Conference, Midland, TX*, March 8–9, 1984.
- [11] J. Fortin, Y. Guéguen, A. Schubnel, Effects of pore collapse and grain crushing on ultrasonic velocities and V-p/V-s, *Journal of Geophysical Research - Solid Earth* (2007)
- [12] D.R. Lide, *Handbook of Chemistry and Physics 1999-2000*, CRC Press, 1999.
- [13] J. Fortin, A. Schubnel, Y. Guéguen, Elastic waves velocities and permeability evolution during compaction of Bleurswiller sandstone, *International Journal of Rock Mechanics and Mining Sciences* 42 (2005) 873-889.
- [14] A. Schubnel, J. Fortin, L. Burlini and Y. Guéguen, Damage and recovery of calcite rocks deformed in the cataclastic regime, *Geological Society of London, special publication ed: Bruhn D. & Burlini L.*, vol. 245, (2005) 203-221.
- [15] J. Corvisier, F. Brunet, A. Fabbri, S. Bernard, N. Findling, G. Rimmelé, V. Barlet-Gouédard, O. Beyssac, B. Goffé, Raman mapping and numerical simulation of calcium carbonates distribution in experimentally carbonated Portland cement cores, *Submitted to European Journal of Mineralogy*, 2009.

[16] J.B. Walsh, The effect of cracks on compressibility of rocks, *Journal of Geophysical Research* 70(2) (1965) 381-389.

[17] G.Mavko, T.Mukerji, J.Dvorkin, in: *The rock physics handbook*, Cambridge University Press, (1998), Cambridge USA.

[18] J.C. Jaeger, N.G.W. Cook and R.W.Zimmerman, in: *Fundamentals of Rock Mechanics* 4th edition, Blackwell publishing (2007), Oxford UK.

[19] V. Baroghel-Bouny, M. Thiery, F. Barberon, G. Villain, Assessment of transport properties of cementitious materials: a major challenge as regards durability?, *European Journal of Environmental and Civil Engineering*, vol.11/6, (2007) 671-696.

[20] A. Fabbri, J. Corvisier, A. Schubnel, F. Brunet, J. Fortin, B. Goffé, V. Barlet-Gouédard, G. Rimmele, Y. Leroy, Effect of carbonation on the hydro-mechanical properties of Portland cements, *Proceedings of the 3rd International Conference on coupled T-H-C-M processes in Geo-Systems*, 2008.

[21] J.W. Carey, J.W. Wigand, M., Chipera, S., *et al* (2007) Analysis and performance of oil well cement with 30 years of CO₂ exposure from the SACROC unit, West Texas, USA, *International Journal of Greenhouse Gas Control*, 75-85. doi:10.1016/S1750-5836(06)00004-1.

[22] P. Benson, A. Schubnel, S. Vinciguerra, C. Trovato, P. Meredith and R.P. Young, Modelling the permeability evolution of micro-cracked rocks from elastic wave velocity inversion at elevated hydrostatic pressure, *Journal of Geophysical Research*, vol.111, (2006) Art. No. B04202.

[23] P.Benson, P. Meredith and A.Schubnel Examining the role of void space fabric in the permeability development of crustal rock with pressure, *Journal of Geophysical Research*, 111, (2006) Art. No. B12203.

Tables caption

Table 1: Sample characterisation.

Table 2: Hydro-mechanical properties of the hardened cement pastes. u stands for 10^{-18} m^2

Figures caption:

Figure 1: Schematic representation of the experimental set-up used for cement carbonation.

Figure 2: Schematic representation of the specimen set-up. Strain gauges are represented in black and the piezoelectric transducers in light grey. V_p stands for compressional waves while V_{sh} and V_{sv} stand for respectively the horizontal and vertical shear waves.

Figure 3: Evolution of the AC and HC sample carbonation front versus the square of carbonation time.

Figure 4: Scanning electron microscope images (Back-Scattered Electron) of (A) the carbonated zone of the sample P51w (1: SiO_2 , 2: C_4AF and 3: $\text{CSH}+\text{CaCO}_3$) and (B) the sample P35d (1: SiO_2 , 2: C_4AF and 3: $\text{CSH}+\text{CaCO}_3$).

Figure 5 : XRPD data for the HC sample P35d (CAF : C_4AF , P : portlandite, Cc : calcite and Ar : aragonite).

Figure 6: Evolution of (A) P and S waves velocities, (B) bulk modulus, (C) shear modulus and (D) cracks density versus the confining pressure $\Sigma(\text{c})$. PO corresponds to the non carbonated samples, black thick lines to HC samples and grey thin lines to AC samples.

Figure 7: $\sigma_d-\varepsilon_{zz}$ (A,B) and $\varepsilon_{\theta\theta}-\varepsilon_{zz}$ (C,D) experimental curves during the deviatoric load of dry samples. To increase the graph readability the curves are artificially shifted.

Figure 8: (A) Water permeability evolution versus deviatoric stress and (B) views on cement samples after fracturing at the end of the tri-axial test.

Table 1

	AC/ HC	t_c days	ϕ %	ρ_d g/cm ³	e_c mm
P0	-	0	41	1.53	-
P13 _w	AC	13	33	1.80	5
P35 _w	AC	35	29	1.90	8
P51 _w	AC	51	28	1.95	10
P62 _w	AC	62	31	1.87	11
P35 _d	HC	35	26	1.99	-
P62 _d	HC	62	24	2.03	-

Table 2

	AC/ HC	E_d GPa	ν_d -	E_u GPa	ν_u -	E_w GPa	ν_w -	κ_{ar} u	κ_w u	f_{rupt} MPa
P0	-	17.5	0.19	16.1	0.29	16.4	0.24	7.1	1.0	63
P13w	AC	21.5	0.20	19.0	0.29	17.4	-	5.2	2.4	50
P35w	AC	19.0	0.20	18.5	0.31	13.4	0.18	3.3	1.3	57
P51w	AC	19.1	0.22	20.6	0.30	-	-	-	-	-
P62w	AC	17.8	0.30	18.8	0.31	15.4	0.33	1.7	0.7	48
P35d	HC	23.0	0.21	20.5	0.32	19.9	0.28	1.4	0.2	80
P62d	HC	37.3	0.24	21.1	0.33	26.6	0.32	-	52	57

Figure 1 :

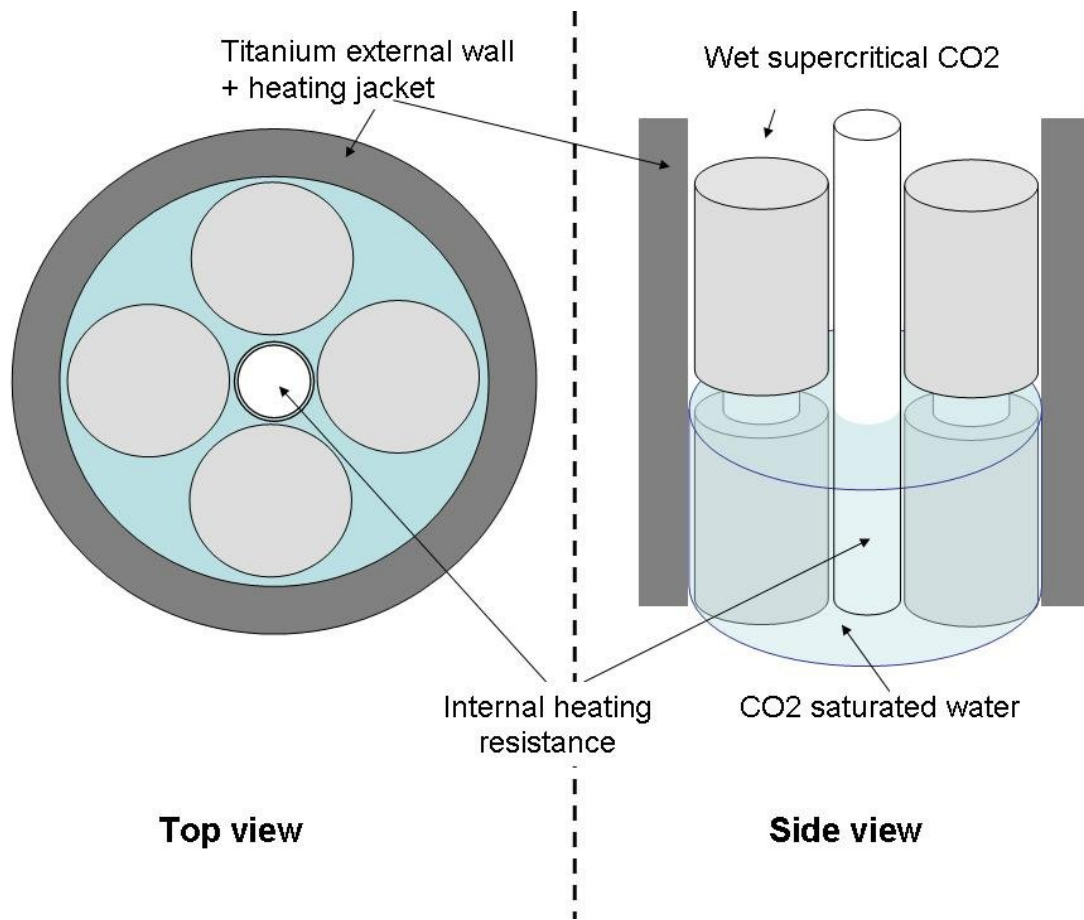


Figure 2

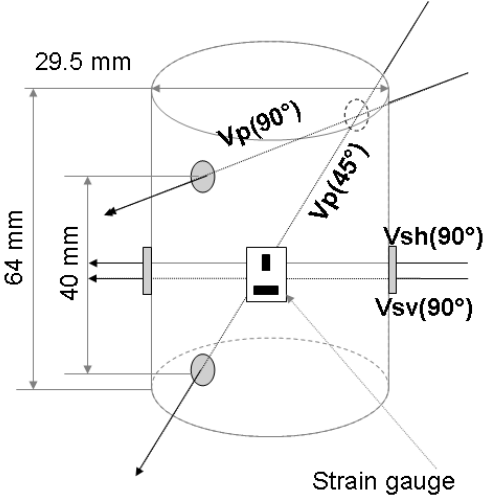


Figure 3 :

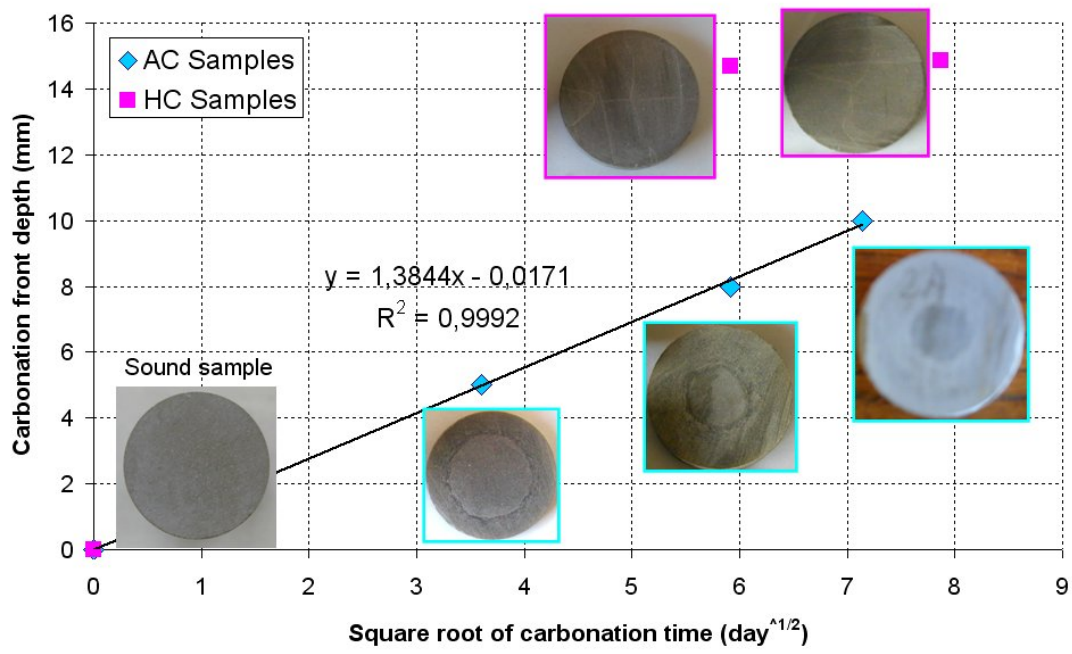


Figure 4

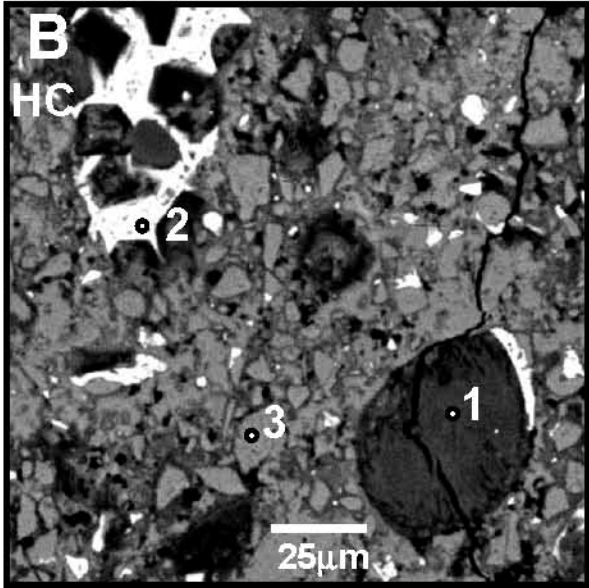
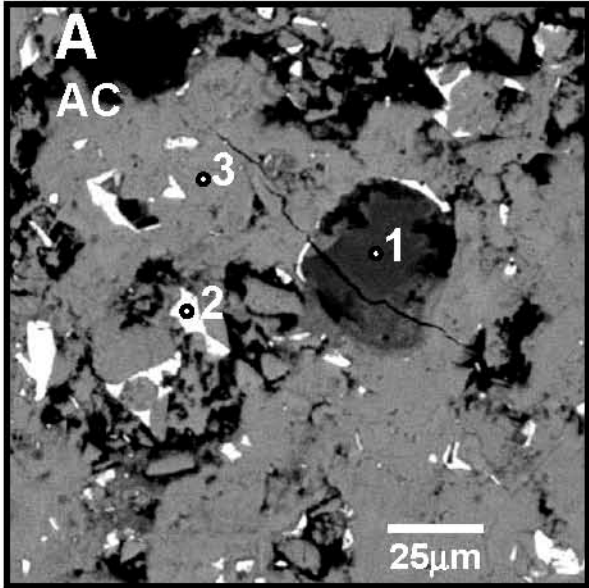


Figure 5

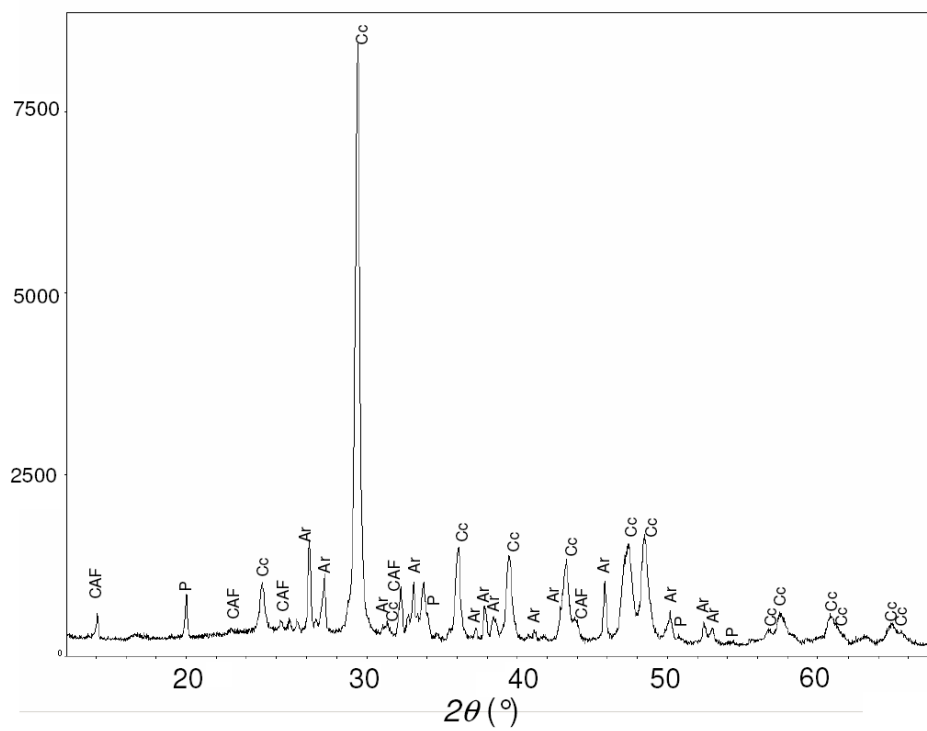


Figure 6

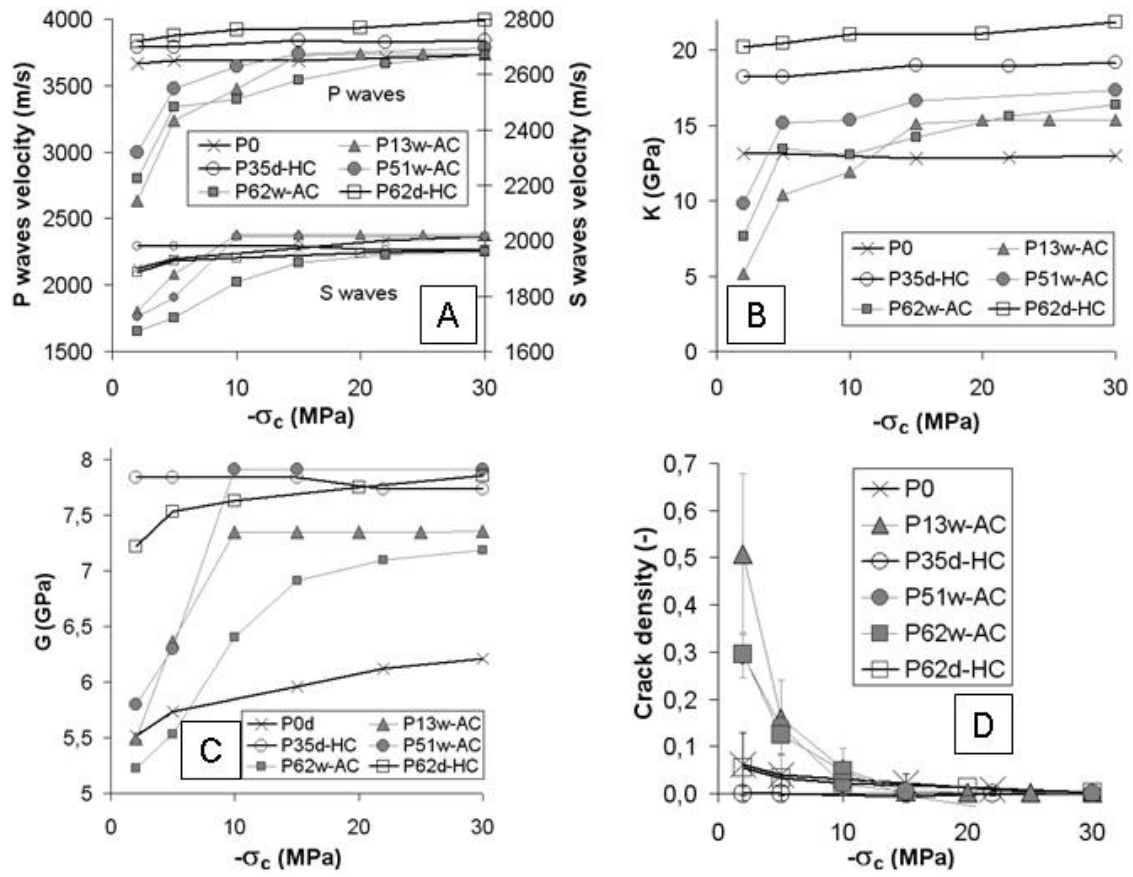


Figure 7

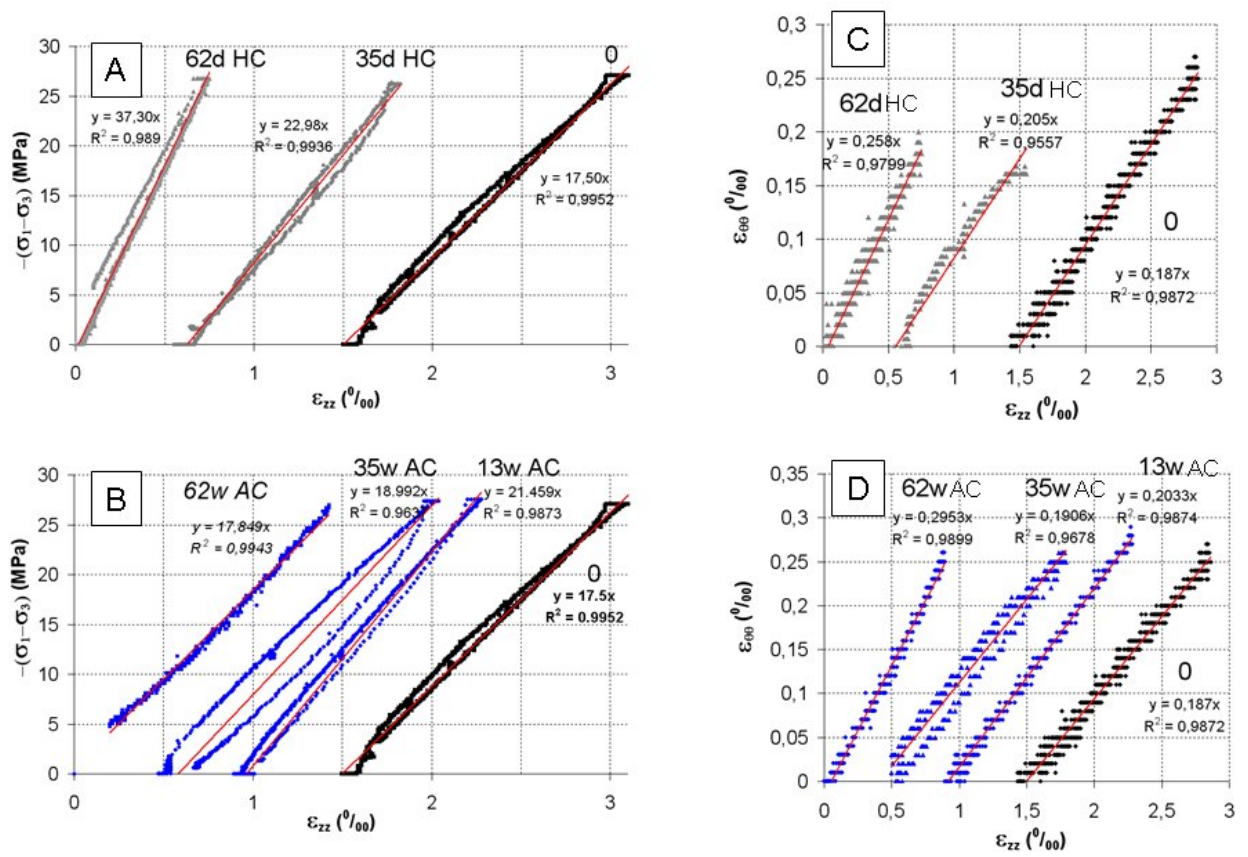


Figure 8

